

Constraint result to the self-interacting dark matter particle mass from the observational data

YIXUAN ZHU¹

¹*Department of Astronomy, Beijing Normal University, Beijing 100875, China*

ABSTRACT

1. INTRODUCTION

The standard Λ -Cold Dark Matter (Λ CDM) model has been successful in explaining the accelerated expansion of the Universe (Riess et al. (1998); Perlmutter et al. (1999)), from the cosmic microwave background (CMB) anisotropies (Bennett et al. (1996)) to the measurement of baryon acoustic oscillations (BAO; Eisenstein et al. (2005)). However, there are also many alternative models that have been proposed to describe the phenomenon, such as the canonical “quintessence” scalar field theories (Ratra & Peebles (1988); Wetterich (1988); Caldwell et al. (1998)), non-canonical “k-essence” theories (Armendariz-Picon et al. (2000, 2001)) and the modified gravity models (see, e.g., Clifton et al. (2012) for a review).

It has been shown that dark matter self-interaction could contribute to the accelerated expansion without dark energy component (Zimdahl et al. (2001); Balakin et al. (2003)). According to the Boltzmann formalism, the disequilibrium between dark matter particle creation and annihilation processes would create an effective source term making negative pressure just like the dark energy. Basilakos & Plionis (2009) investigated the analytical solutions for the simple interacting dark matter (IDM) model, and find that the effective annihilation term is much smaller than the results given by the general methods. The gravitational matter creation model (Lima et al. (2008)) is mathematically equivalent to one case of the IDM models (Basilakos & Plionis (2009)).

In this paper, we use the newly revised data from $H(z)$, supernovae Ia and baryon acoustic oscillation by using the Markov chain Monte Carlo (MCMC) method. The constraint result gives an upper limit for the linear ratio between the dark matter annihilation cross section $\langle\sigma v\rangle$ and the dark matter particle mass M_χ about $9 \times 10^{-15} \text{ cm}^3 \text{ s}^{-1} \text{ GeV}^{-1}$.

The paper is arranged as follows: In Sec.2, we review the basic equations in the IDM model, in Sec.3, we introduce the observational datasets used in this analysis, in Sec.4, we give the constraint results of the IDM model and compare our results with other relevant dark matter constraints, and finally we conclude in Sec.5.

2. THE BASIC EQUATIONS IN THE IDM MODEL

We assume that the total density of the cosmic fluid obeys the collisional Boltzmann equation (Kolb & Turner (2019))

$$\dot{\rho} + 3H\rho + \kappa\rho^2 - 2\Psi = 0, \quad (1)$$

where ρ is the total energy-density of the cosmic fluid, containing dark matter, baryons, and any type of exotic energy, Ψ is the rate of creation of DM particle pairs, and the annihilation parameter $\kappa(\geq 0)$ is given by:

$$\kappa = \frac{\langle\sigma v\rangle}{M_\chi}, \quad (2)$$

where σ is the cross section for annihilation, v is the mean particle velocity, and M_χ is the mass of the DM particle. Compared to the usual fluid equation, the effective pressure term is

$$P = \frac{\kappa\rho^2 - \Psi}{3H}. \quad (3)$$

When $\kappa\rho^2 - \Psi < 0$, what means that the IDM particle creation term is larger than the annihilation item, IDM may serve as a negative pressure source in the global dynamics of the Universe, like the role of Dark Energy in the general cosmological models.

Basilakos & Plionis (2009) identified two functional forms for which the previous Boltzmann equation can be solved analytically. Referring to Appendix B in Basilakos & Plionis (2009), only one of these two is of interest because it provides a “ $\propto \alpha^{-3}$ ” dependence of the scale factor, which is

$$\Psi(\alpha) = \alpha H(\alpha) R(\alpha) = C_1(n+3)\alpha^n H(\alpha) + \kappa C_1^2 \alpha^{2m}. \quad (4)$$

And the total energy density is

$$\rho(\alpha) = C_1 \alpha^n + \frac{\alpha^{-3} F(\alpha)}{C_2 - \int_1^\alpha x^{-3} f(x) F(x) dx}, \quad (5)$$

where $f(\alpha) = -\kappa/[\alpha H(\alpha)]$, and the kernel function $F(\alpha)$ has the form

$$F(\alpha) = \exp \left[-2\kappa C_1 \int_1^\alpha \frac{x^{n-1}}{H(x)} dx \right]. \quad (6)$$

The first term of Eq.(5) is the density corresponding to the residual matter creation that results from a possible disequilibrium between the particle creation and annihilation processes, while the second term can be viewed as the energy density of the self-IDM particles that are dominated by the annihilation process.

2.1. Model 1: relation to the Λ CDM model

If $n = 0$, the global density evolution can be transformed as

$$\rho(\alpha) = C_1 + \alpha^{-3} \frac{e^{-2\kappa C_1(t-t_0)}}{C_2 + \kappa Z(t)}, \quad (7)$$

where $Z(t) = \int_{t_0}^t \alpha^{-3} e^{-2\kappa C_1(t'-t_0)} dt'$ (Basilakos & Plionis (2009)). Using the usual unit-less Ω -like parameterization, we obtain that

$$\left(\frac{H}{H_0}\right)^2 = \Omega_{1,0} + \frac{\Omega_{1,0}\Omega_{2,0}\alpha^{-3}e^{-2\kappa C_1(t-t_0)}}{\Omega_{1,0} + \kappa C_1\Omega_{2,0}Z(t)}, \quad (8)$$

where $\Omega_{1,0} = 8\pi G C_1 / 3H_0^2$ and $\Omega_{2,0} = 8\pi G / 3H_0^2 C_2$, which related to Ω_Λ and Ω_m in the Λ CDM model, respectively. From Eq.(2), we can also give the mass of the DM particle related to the range of κC_1 (in the unit of Gyr^{-1})

$$M_\chi = \frac{3.325 \times 10^{-12}}{\kappa C_1} \frac{\langle \sigma v \rangle}{10^{-23}} h^2 (1 - \Omega_{2,0}) \text{ GeV}, \quad (9)$$

where $h \equiv H_0 / [100 \text{ km/s/Mpc}]$.

2.2. Model 2 : relation to the w CDM model

If $n \neq 0$, the global density evolution is Eq.(5), and the usual unit-less Ω -like can be written as

$$\left(\frac{H}{H_0}\right)^2 = \Omega_{1,0}\alpha^n + \frac{\Omega_{1,0}\Omega_{2,0}\alpha^{-3}F(\alpha)}{\Omega_{1,0} + \kappa C_1\Omega_{2,0} \int_1^\alpha \frac{F(x)}{x^4 H(x)} dx}, \quad (10)$$

where $\Omega_{1,0}$ and $\Omega_{2,0}$ are the same defined as Eq.(8), and $F(\alpha)$ is given by Eq.(6).

Considering the limit of $\kappa \rightarrow 0$, the global density evolution can be simplified as

$$\rho(\alpha) = C_1 a^n + \frac{1}{C_2} a^{-3}, \quad (11)$$

and Eq.(10) becomes

$$\left(\frac{H}{H_0}\right)^2 = \Omega_{1,0}\alpha^n + \Omega_{2,0}\alpha^{-3}. \quad (12)$$

The conditions $n > 2$ indicates that the IDM model has an inflection point (Basilakos & Plionis (2009)), and we define $w_{\text{IDM}} = -1 - n/3$ as the equation of state (EoS) of the IDM model. This solution is mathematically equivalent to that of the gravitational matter creation model of Lima et al. (2008).

3. DATASET

To constrain the relevant IDM models (Basilakos & Plionis (2009)), we use the newly revised observational $H(z)$ data (OHD) (Simon et al. (2005); Stern et al. (2010); Moresco et al. (2012); Zhang et al. (2014); Moresco et al. (2016); Ratsimbazafy et al. (2017); Moresco (2015); Borghi et al. (2022); Jiao et al. (2023)), the Pantheon+ set of 1701 SNe Ia (Scolnic et al. (2022)), the BAO data from SDSS-IV (Alam et al. (2021)) and DESI DR2 (Collaboration et al. (2025)).

3.1. The observational $H(z)$ data

It is widely known that the Hubble parameter $H(z)$ depends on the differential age as a function of redshift z in the form

$$H(z) = -\frac{1}{1+z} \frac{dz}{dt}, \quad (13)$$

which provides a direct measurement on $H(z)$ based on dz/dt . OHD measurements have recently been acquired mainly employing cosmic chronometers (CC). The CC method is used to provide 33 observational data points, which are taken in the redshift range $[0.07, 1.965]$. The Table 1 lists the OHD dataset used in this analysis. In this case, χ^2 can be defined as

$$\chi_{\text{OHD}}^2 = \sum_i \frac{(H_{\text{th}} - H_{\text{data}})^2}{\sigma_i^2}. \quad (14)$$

3.2. Type Ia supernovae

SNe Ia have long been used as “standard candles” to give a direct measurement of their luminosity distance, and provides strong constraints on cosmological parameters. We use the latest Pantheon+ data set of 1701 SNe Ia samples (Scolnic et al. (2022)), which covers the redshift range $[0, 2.26]$.

The χ^2 of SNe Ia can be defined as

$$\chi_{\text{SNe}}^2 = \Delta C^{-1} \Delta^T - \frac{B^2}{C} + \ln \left(\frac{C}{2\pi} \right), \quad (15)$$

where $\Delta = (\mu_{\text{th}} - \mu_{\text{data}})$, C^{-1} is the inverse of the covariance matrix of the SNe Ia data, B is the sum of ΔC^{-1} and C is the sum of C^{-1} , the distance modulus is $\mu = 5 \log_{10}(d_L/\text{Mpc}) + 25$, and the luminosity distance d_L can be given as a function of redshift z

$$d_L = (1+z) \int_0^z \frac{cdz'}{H(z')}. \quad (16)$$

3.3. Baryon acoustic oscillation

The Baryon acoustic oscillation (BAO) method provides a key cosmological probe sensitive to the cosmic

z	$H(z)$	Reference
0.07	69 ± 19.6	Zhang et al. (2014)
0.09	69 ± 12	Simon et al. (2005)
0.12	68.6 ± 26.2	Zhang et al. (2014)
0.17	83 ± 8	Simon et al. (2005)
0.179	75 ± 4	Moresco et al. (2012)
0.199	75 ± 5	Moresco et al. (2012)
0.2	72.9 ± 29.6	Zhang et al. (2014)
0.27	77 ± 14	Simon et al. (2005)
0.28	88.8 ± 36.6	Zhang et al. (2014)
0.352	83 ± 14	Moresco et al. (2012)
0.3802	83 ± 13.5	Moresco et al. (2016)
0.4	95 ± 17	Simon et al. (2005)
0.4004	77 ± 10.2	Moresco et al. (2016)
0.4247	87.1 ± 11.2	Moresco et al. (2016)
0.4497	92.8 ± 12.9	Moresco et al. (2016)
0.47	89 ± 34	Ratsimbazafy et al. (2017)
0.4783	80.9 ± 9	Moresco et al. (2016)
0.48	97 ± 62	Stern et al. (2010)
0.593	104 ± 13	Moresco et al. (2012)
0.68	92 ± 8	Moresco et al. (2012)
0.75	98.8 ± 33.6	Borghi et al. (2022)
0.781	105 ± 12	Moresco et al. (2012)
0.8	113.1 ± 15.1	Jiao et al. (2023)
0.875	125 ± 17	Moresco et al. (2012)
0.88	90 ± 40	Stern et al. (2010)
0.9	117 ± 23	Simon et al. (2005)
1.037	154 ± 20	Moresco et al. (2012)
1.3	168 ± 17	Simon et al. (2005)
1.363	160 ± 33.6	Moresco (2015)
1.43	177 ± 18	Simon et al. (2005)
1.53	140 ± 14	Simon et al. (2005)
1.75	202 ± 40	Simon et al. (2005)
1.965	186.5 ± 50.4	Moresco (2015)

Table 1. The OHD dataset from different reference.

expansion history with well-controlled systematics. We use two BAO datasets from the SDSS-IV (Alam et al. (2021)) and DESI DR2 (Collaboration et al. (2025)), which are given at Table 2 respectively. The redshift is up to 2.33 both in the SDSS and the DESI 2024 dataset.

The χ^2 function for the BAO data is defined as

$$\chi_{\text{BAO}}^2 = \sum_i \frac{(D_{\text{th}}/r_d - D_{\text{data}}/r_d)^2}{\sigma_i^2}, \quad (17)$$

where D refers to D_{M} , D_{H} , or D_{V} , which are given as

$$D_{\text{M}}(z) = c \int_0^z \frac{dz'}{H(z')}, \quad (18)$$

$$D_{\text{H}}(z) = \frac{c}{H(z)}, \quad (19)$$

$$D_{\text{V}}(z) = \left[\frac{c}{H(z)} D_{\text{M}}(z) D_{\text{H}}(z) \right]^{1/3}, \quad (20)$$

and r_d is the sound horizon at the drag epoch, which is given as

$$r_d = \int_{z_{\text{drag}}}^{\infty} \frac{c_s(z') dz'}{H(z')}, \quad (21)$$

where c_s is the sound speed prior to recombination.

Mathematically, the solution of Eq.(8) will encounter the singularity at the upper limit of the redshift z_{max} (see Appendix), and the cross parameter $r_d h$ is used to give the constraints.

4. CONSTRAINT RESULTS AND DISCUSSION

4.1. Constraint results to the IDM model

We use the Markov chain Monte Carlo (MCMC) method based on the opening package `emcee` to give a global constraints to the free parameters $\Omega_{2,0}$ and $\log_{10}(\kappa C_1)$ in Model 1 and n in Model 2. The prior range set for free parameters are given at Table 3.

The Eq.(8) convergent to the flat Λ CDM model as $\log_{10}(\kappa C_1) \rightarrow -\infty$, thus the constraints could only give the upper limit of what, and we use the 95% quantiles to determine the upper bounds of the parameters. The constraint results are shown in Figure 1-3 and summarized in Table 4.

For the dataset which cannot give a constraint to H_0 , we use $h \simeq 0.7$ as the default value to calculate the annihilation parameter κ .

4.2. Compared with other results

The SNe Ia dataset gives a value $\Omega_{2,0} \simeq 0.38$. The constraint result to Pantheon+ SNe Ia dataset in the flat Λ CDM model is $\Omega_m \simeq 0.33$ (Borghi et al. (2022)),

5. CONCLUSIONS

APPENDIX

Dataset/Tracer	z_{eff}	D_V/r_d	D_M/r_d	D_H/r_d
SDSS-IV				
MGS	0.15	4.51 ± 0.14	—	—
BOSS galaxy	0.38	—	10.27 ± 0.15	24.89 ± 0.58
BOSS galaxy	0.51	—	13.38 ± 0.18	22.43 ± 0.48
eBOSS LRG	0.70	—	17.65 ± 0.30	19.78 ± 0.46
eBOSS ELG	0.85	—	19.5 ± 1.0	19.6 ± 2.1
eBOSS quasar	1.48	—	30.21 ± 0.79	13.23 ± 0.47
Ly α -Ly α	2.33	—	37.6 ± 1.9	8.93 ± 0.28
Ly α -quasar	2.33	—	37.3 ± 1.7	9.08 ± 0.34
DESI DR2				
BGS	0.295	7.942 ± 0.075	—	—
LRG1	0.510	12.720 ± 0.099	13.588 ± 0.167	21.863 ± 0.425
LRG2	0.706	16.050 ± 0.110	17.351 ± 0.177	19.455 ± 0.330
LRG3+ELG1	0.934	19.721 ± 0.091	21.576 ± 0.152	17.641 ± 0.193
ELG2	1.321	24.252 ± 0.174	27.601 ± 0.318	14.176 ± 0.221
QSO	1.484	26.055 ± 0.398	30.512 ± 0.760	12.817 ± 0.516
Ly α	2.330	31.267 ± 0.256	38.988 ± 0.531	8.632 ± 0.101
LRG3	0.922	19.656 ± 0.105	21.648 ± 0.178	17.577 ± 0.213
ELG1	0.955	20.008 ± 0.183	21.707 ± 0.335	17.803 ± 0.297

Table 2. The BAO+RSD measurements dataset from SDSS-IV and DESI DR2.

parameter	initial	prior
$\Omega_{2,0}$	0.3	$\mathcal{U}[0.0, 1.0]$
$\log_{10}(\kappa C_1/\text{Gyr}^{-1})$	—	$\mathcal{U}[-10, 0]$
n	0	$\mathcal{U}[-5, 5]$
$H_0[\text{km}/(\text{s}\cdot\text{Mpc})]$	70	$\mathcal{U}[60, 80]$
$r_d h[\text{Mpc}]$	100	$\mathcal{U}[50, 150]$

Table 3. Parameters and priors used in analysis. All of the priors are flat in the ranges given. The $\log_{10}(\kappa C_1)$ does not have a predicted value, and the initial value of each chain is selected randomly uniformly within the prior range.

Model/Dataset	$\Omega_{2,0}$	$\log_{10}(\kappa C_1/\text{Gyr}^{-1})$	$10^{15}\kappa[\text{cm}^3/(\text{s}\cdot\text{GeV})]$	n	w_{IDM}
Model 1					
SNe Ia	0.380 ± 0.020	< -3.05	< 8.82	—	—
BAO	0.2980 ± 0.0070	< -3.66	< 1.91	—	—
BAO + SNe Ia + OHD	$0.3079^{+0.0051}_{-0.0067}$	< -3.99	< 0.907	—	—
Model 2 ($\kappa = 0$)					
SNe Ia	$0.215^{+0.10}_{-0.073}$	—	—	$-0.82^{+0.29}_{-0.45}$	$-0.73^{+0.15}_{-0.10}$
BAO	0.2952 ± 0.0073	—	—	$-0.29^{+0.15}_{-0.18}$	$-0.90^{+0.06}_{-0.05}$
BAO + SNe Ia + OHD	0.2945 ± 0.0075	—	—	-0.42 ± 0.11	-0.86 ± 0.04
Model 2 ($\kappa \neq 0$)					
SNe Ia	$0.143^{+0.067}_{-0.11}$	< -2.15	< 50.7	$-1.17^{+0.17}_{-0.35}$	$-0.61^{+0.12}_{-0.06}$
BAO	$0.287^{+0.017}_{-0.0022}$	< -2.44	< 31.3	$-0.34^{+0.22}_{-0.17}$	$-0.89^{+0.06}_{-0.07}$
BAO + SNe Ia + OHD	0.241 ± 0.062	< -1.90	< 101.8	$-0.73^{+0.33}_{-0.24}$	$-0.76^{+0.08}_{-0.11}$

Table 4. The constraint results of the IDM model.

Figure 1. The constraint result from the supernovae Ia data (left), the BAO data (middle) and the BAO + SNe Ia + OHD data (right).

Figure 2. The constraint result from the supernovae Ia data (left), the BAO data (middle) and the BAO + SNe Ia + OHD data (right).

A. THE THEORETICAL SOLUTION OF MODEL 1

Apply the Eq.(12) to Eq.(8), we can get a simple nonlinear second-order differential equation for the redshift $z(t)$, which can be written as

$$2H_0^2\Omega_{1,0}(1+z)^2z'z'' + \kappa C_1z'^4 - 5H_0^2\Omega_{1,0}(1+z)z'^3 + 3H_0^4\Omega_{1,0}^2(1+z)^3z' - H_0^4\Omega_{1,0}^2\kappa C_1[(z+1)^4 - 1] = H_0^4\Omega_{1,0}^2\kappa C_1, \quad (\text{A1})$$

where the prime denotes the derivative with respect to t . The equation can be simplified as

$$2H_0^2\Omega_{1,0}y^2y'y'' + \kappa C_1y'^4 - 5H_0^2\Omega_{1,0}yy'^3 + 3H_0^4\Omega_{1,0}^2y^3y' - H_0^4\Omega_{1,0}^2\kappa C_1y^4 = 0, \quad (\text{A2})$$

where $y = z + 1$, now it is a homogeneous function and we can give the general solution as $y = \exp f$ with f a function of t , the equation now is

$$2H_0^2\Omega_{1,0}f'f'' + \kappa C_1f'^4 - 3H_0^2\Omega_{1,0}f'^3 + 3H_0^4\Omega_{1,0}^2f' - H_0^4\Omega_{1,0}^2\kappa C_1 = 0. \quad (\text{A3})$$

We use $g = f'$, which also gives $g(t) = y'/y = -H(t)$, then the equation can be written as

$$2H_0^2\Omega_{1,0}gg' + \kappa C_1g^4 - 3H_0^2\Omega_{1,0}g^3 + 3H_0^4\Omega_{1,0}^2g - H_0^4\Omega_{1,0}^2\kappa C_1 = 0. \quad (\text{A4})$$

It can be theoretically solved and the solution has a form like

$$g(t) = \mathcal{G}\left(-\frac{t}{2H_0^2\Omega_{1,0}} + \text{Const}\right), \quad (\text{A5})$$

where \mathcal{G} is the inverse function of

$$\mathcal{F}(x) = \frac{3H_0\sqrt{\Omega_{1,0}}\text{arctanh}\frac{x}{H_0\sqrt{\Omega_{1,0}}} - \kappa C_1\log(x^2 - H_0^2\Omega_{1,0}) + \kappa C_1\log(\kappa C_1x^2 - 3H_0^2\Omega_{1,0}x + H_0^2\Omega_{1,0}\kappa C_1)}{9H_0^4\Omega_{1,0}^2 - 4H_0^2\Omega_{1,0}(\kappa C_1)^2}. \quad (\text{A6})$$

In this term, $\text{arctanh}(x) \doteq \frac{1}{2}\log\left(\frac{x+1}{x-1}\right)$ when $x < -1$, and the Const is determined by the boundary condition $g(0) \rightarrow -\infty$, which is

$$\text{Const} = \mathcal{F}(-\infty) \equiv \lim_{x \rightarrow -\infty} \mathcal{F}(x) = \frac{\kappa C_1 \ln \kappa C_1}{9H_0^4\Omega_{1,0}^2 - 4H_0^2\Omega_{1,0}(\kappa C_1)^2}. \quad (\text{A7})$$

The initial time of today t_0 can be easily given as

$$t_0 = 2H_0^2\Omega_{1,0}[\mathcal{F}(-\infty) - \mathcal{F}(-H_0)], \quad (\text{A8})$$

and the redshift z_{\max} can be calculated as

$$z_{\max} = \exp\left[2H_0^2\Omega_{1,0}\int_{-\infty}^{-H_0}[\mathcal{F}(-\infty) - \mathcal{F}(x)]dx + H_0t_0\right] - 1, \quad (\text{A9})$$

and z_{\max} is also a function of $\Omega_{2,0}$, κC_1 and H_0 .

REFERENCES

- | | |
|--|---|
| <p>Alam, S., Aubert, M., Avila, S., et al. 2021, Phys. Rev. D, 103, 083533, doi: 10.1103/PhysRevD.103.083533</p> | <p>Armendariz-Picon, C., Mukhanov, V., & Steinhardt, P. J. 2000, Phys. Rev. Lett., 85, 4438, doi: 10.1103/PhysRevLett.85.4438</p> |
|--|---|

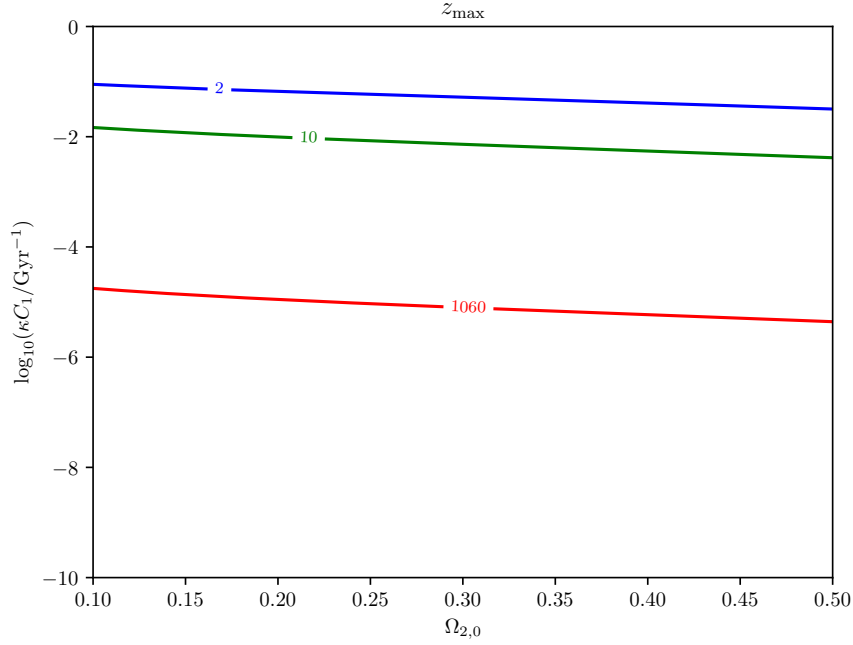


Figure 3. The redshift z_{max} as $H_0 = 70$ km/s/Mpc

- . 2001, Phys. Rev. D, 63, 103510, doi: [10.1103/PhysRevD.63.103510](https://doi.org/10.1103/PhysRevD.63.103510)
- Balakin, A. B., Pavón, D., Schwarz, D. J., & Zimdahl, W. 2003, New Journal of Physics, 5, 85, doi: [10.1088/1367-2630/5/1/385](https://doi.org/10.1088/1367-2630/5/1/385)
- Basilakos, S., & Plionis, M. 2009, A&A, 507, 47, doi: [10.1051/0004-6361/200912661](https://doi.org/10.1051/0004-6361/200912661)
- Bennett, C. L., Banday, A. J., Górski, K. M., et al. 1996, The Astrophysical Journal, 464, L1, doi: [10.1086/310075](https://doi.org/10.1086/310075)
- Borghi, N., Moresco, M., & Cimatti, A. 2022, The Astrophysical Journal Letters, 928, L4, doi: [10.3847/2041-8213/ac3fb2](https://doi.org/10.3847/2041-8213/ac3fb2)
- Caldwell, R. R., Dave, R., & Steinhardt, P. J. 1998, Phys. Rev. Lett., 80, 1582, doi: [10.1103/PhysRevLett.80.1582](https://doi.org/10.1103/PhysRevLett.80.1582)
- Clifton, T., Ferreira, P. G., Padilla, A., & Skordis, C. 2012, Physics Reports, 513, 1, doi: <https://doi.org/10.1016/j.physrep.2012.01.001>
- Collaboration, D., Abdul-Karim, M., Aguilar, J., et al. 2025, DESI DR2 Results II: Measurements of Baryon Acoustic Oscillations and Cosmological Constraints. <https://arxiv.org/abs/2503.14738>
- Eisenstein, D. J., Zehavi, I., Hogg, D. W., et al. 2005, The Astrophysical Journal, 633, 560, doi: [10.1086/466512](https://doi.org/10.1086/466512)
- Jiao, K., Borghi, N., Moresco, M., & Zhang, T.-J. 2023, The Astrophysical Journal Supplement Series, 265, 48, doi: [10.3847/1538-4365/acbc77](https://doi.org/10.3847/1538-4365/acbc77)
- Kolb, E. W., & Turner, M. S. 2019, The Early Universe, Vol. 69 (Taylor and Francis), doi: [10.1201/9780429492860](https://doi.org/10.1201/9780429492860)
- Lima, J. A. S., Silva, F. E., & Santos, R. C. 2008, Classical and Quantum Gravity, 25, 205006, doi: [10.1088/0264-9381/25/20/205006](https://doi.org/10.1088/0264-9381/25/20/205006)
- Moresco, M. 2015, Monthly Notices of the Royal Astronomical Society: Letters, 450, L16, doi: [10.1093/mnrasl/slv037](https://doi.org/10.1093/mnrasl/slv037)
- Moresco, M., Cimatti, A., Jimenez, R., et al. 2012, Journal of Cosmology and Astroparticle Physics, 2012, 006, doi: [10.1088/1475-7516/2012/08/006](https://doi.org/10.1088/1475-7516/2012/08/006)
- Moresco, M., Pozzetti, L., Cimatti, A., et al. 2016, Journal of Cosmology and Astroparticle Physics, 2016, 014, doi: [10.1088/1475-7516/2016/05/014](https://doi.org/10.1088/1475-7516/2016/05/014)
- Perlmutter, S., Aldering, G., Goldhaber, G., et al. 1999, The Astrophysical Journal, 517, 565, doi: [10.1086/307221](https://doi.org/10.1086/307221)
- Ratra, B., & Peebles, P. J. E. 1988, Phys. Rev. D, 37, 3406, doi: [10.1103/PhysRevD.37.3406](https://doi.org/10.1103/PhysRevD.37.3406)
- Ratsimbazafy, A. L., Loubser, S. I., Crawford, S. M., et al. 2017, Monthly Notices of the Royal Astronomical Society, 467, 3239, doi: [10.1093/mnras/stx301](https://doi.org/10.1093/mnras/stx301)
- Riess, A. G., Filippenko, A. V., Challis, P., et al. 1998, The Astronomical Journal, 116, 1009, doi: [10.1086/300499](https://doi.org/10.1086/300499)
- Riess, A. G., Yuan, W., Macri, L. M., et al. 2022, The Astrophysical Journal Letters, 934, L7, doi: [10.3847/2041-8213/ac5c5b](https://doi.org/10.3847/2041-8213/ac5c5b)

- Scolnic, D., Brout, D., Carr, A., et al. 2022, The Astrophysical Journal, 938, 113, doi: [10.3847/1538-4357/ac8b7a](https://doi.org/10.3847/1538-4357/ac8b7a)
- Simon, J., Verde, L., & Jimenez, R. 2005, Phys. Rev. D, 71, 123001, doi: [10.1103/PhysRevD.71.123001](https://doi.org/10.1103/PhysRevD.71.123001)
- Stern, D., Jimenez, R., Verde, L., Kamionkowski, M., & Stanford, S. A. 2010, Journal of Cosmology and Astroparticle Physics, 2010, 008, doi: [10.1088/1475-7516/2010/02/008](https://doi.org/10.1088/1475-7516/2010/02/008)
- Wetterich, C. 1988, Nuclear Physics B, 302, 668, doi: [https://doi.org/10.1016/0550-3213\(88\)90193-9](https://doi.org/10.1016/0550-3213(88)90193-9)
- Zhang, C., Zhang, H., Yuan, S., et al. 2014, Research in Astronomy and Astrophysics, 14, 1221, doi: [10.1088/1674-4527/14/10/002](https://doi.org/10.1088/1674-4527/14/10/002)
- Zimdahl, W., Schwarz, D. J., Balakin, A. B., & Pavón, D. 2001, Phys. Rev. D, 64, 063501, doi: [10.1103/PhysRevD.64.063501](https://doi.org/10.1103/PhysRevD.64.063501)